RESEARCH

Investigation of electrical and dielectric properties of complex perovskite $Gd_{2/3}Cu_3Ti_4O_{12}$ and $Gd_{2/3}Cu_3Ti_{3.95}Co_{0.025}V_{0.025}O_{12}$ ceramic synthesized via novel semi-wet route

Anup Kumar · Harish Verma · Dhanesh Tiwary · K. D. Mandal

Abstract $Gd_{2/3}Cu_3Ti_4O_{12}$ (GCTO) and Co V-doped $Gd_{2/3}Cu_3Ti_4O_{12}$ (GCTCVO) ceramic nano-particles were synthesized by utilizing a cost-effective chemical route. XRD pattern analysis confirms single-phase formation of $Gd_{2/3}Cu_3Ti_4O_{12}$ (GCTO) and Co V-doped $Gd_{2/3}Cu_3Ti_4O_{12}$ (GCTCVO) ceramic. XPS analysis verified the correct oxidation states of various elements. Elemental composition was determined using EDS. The dielectric constant of GCTO ceramic reached its peak at 726, measured at 545 K and 1 kHz, while it reached its peak at 217, measured at 563 K and 1 kHz for GCTCVO. It was also observed that both ceramic show Maxwell relaxation behavior. The tangent loss value of the GCTO and GCTCVO ceramic was noted as 0.08 and 0.13 at 304 K and all measured frequency.

Keywords Chemical route · XRD · EDS · Dielectric properties

Introduction

Such type of material having large dielectric constant has attracted the attention. Since many years, several new materials have attempted to synthesize which possess great dielectric constant. It has always been a requirement of such type of capacitor possessing high dielectric constant for the advancement of capacitor technology. These giant dielectric ceramic materials are very useful to miniaturize capacitor for the requirement of I.C. in different types of electronic devices. [1, 2]

Such type of ceramic materials which possess high dielectric constant and low tan loss but strong dependencies with temperature will not be beneficial for the battery purpose. The recently synthesized ceramic material is environmentally friendly as capacitor material. Multilayer capacitor (MLCC), dynamic random access memory (DRAM), microwave devices, and several electronic devices in different automobile sector are some examples of vital application in our daily life.

A complex perovskite-type ceramic material $CaCu_3Ti_4O_{12}$(CCTO) shows giant dielectric constant and temperature and frequency-independent property. Due to this it is desirable material for the advancement of new microelectronics and memory devices which play very crucial role in miniaturizing the batteries, but it is very unfortunate that it also shows very large dielectric loss, which limits its application. To modify the performance of CCTO ceramic material,

A. Kumar · D. Tiwary · K. D. Mandal (✉)
Department of Chemistry, Indian Institute of Technology (Banaras Hindu University), Varanasi 221005, U.P., India
e-mail: kdmandal.apc@itbhu.ac.in

H. Verma
Department of Physics, Indian Institute of Technology (Banaras Hindu University), Varanasi 221005, U.P., India

different elements are being doped at different sites or at a single site either one by one or simultaneously. [3–5]

Earlier, it has been published that when 2 atomic % Fe was doped at Ti site in dielectric CCTO ceramic, a very big change in dielectric constant was observed [6]. Also, when Mn was substituted on Cu as well as Ti, then a drastic lowering in dielectric constant (ε') was observed and this phenomenon was explained assuming it that the suppression of barrier layer formation on grain boundaries [7, 8]. When Sn was substituted on titanium sites, dielectric constant (ε') as well as dielectric loss (tan δ) was reduced to a great extent [9]. An appreciable lowering in tangent loss was observed without any more changes in dielectric constant when 2 mol % cesium was introduced on calcium sites [10].

Similarly, we conducted a comprehensive investigation on $SrCu_3Ti_4O_{12}$ (SCTO), $La_{2/3}Cu_3Ti_4O_{12}$ (LCTO), and $Bi_{2/3}Cu_3Ti_4O_{12}$ (BCTO) ceramics to gain a systematic understanding of the dielectric properties of oxides structurally similar to $CaCu_3Ti_4O_{12}$, along with the associated mechanisms. Surprisingly, contrary to previous literature findings, we observed a remarkable giant dielectric permittivity effect in all of these ceramics, with ε' values exceeding $1.5 \times 10.^4$ at low frequencies. Additionally, the presence of a CuO secondary phase was confirmed in these materials. In essence, our results can be described by the analogous mechanism of the internal barrier layer capacitance effect, as previously proposed for $CaCu_3Ti_4O_{12}$ ceramics. This suggests that the occurrence of giant ε' phenomena is likely to be a common trait within the broader family of oxides sharing both structural and compositional similarities with $CaCu_3Ti_4O_{12}$.[11]

In many chemical processes, achieving high temperatures and procuring expensive raw materials are essential. However, in the current study, we employ an innovative semi-wet route method to comparatively investigate $Gd_{2/3}Cu_3Ti_4O_{12}$ (GCTO) and $Gd_{2/3}Cu_3Ti_4O_{12}$ doped with cobalt and vanadium (GCTCVO) at titanium sites, all at relatively low temperatures. This cost-effective novel semi-wet route utilizes a citrate nitrate gel chemical method with TiO_2 instead of the costly titanium isopropoxide as the raw material. We conducted various characterization techniques, including powder XRD, SEM, XPS, dielectric studies, and impedance analysis, to study the samples in detail.

Experimental

Material synthesis

The synthesis of $Gd_{2/3}Cu_3Ti_4O_{12}$ (GCTO) and $Gd_{2/3}Cu_3Ti_4O_{12}$ ceramics doped with cobalt and vanadium (GCTCVO) was accomplished through a semi-wet method. High-quality chemicals, including gadolinium oxide Gd_2O_3 (Aldrich, Sigma, 99.9%), copper acetate mono-hydrate Cu $(CH_3COO)_2 \cdot H_2O$ (98% Merck, India), and titanium oxide TiO_2 (98.5% Merck, India), were employed in stoichiometric proportions. The procedure began by dissolving Gd_2O_3 and Cu $(CH_3COO)_2 \cdot H_2O$ in distilled water, followed by the addition of the required amount of solid TiO_2 to this solution. This solution was then mixed with the appropriate quantity of citric acid (99.5%, Merck India). Using a hot-plate magnetic stirrer, the mixture was heated thoroughly and stirred at a temperature range of 343–353 K, causing the water to evaporate and enabling self-ignition. Once the major portion of the gases was removed, dry ceramic powder was obtained.

The resulting GCTO powder was further crushed with a mortar pestle to achieve an extremely fine consistency. These powdered samples were subsequently subjected to calcination at 1073 K for 6 h. Pellets having cylindrical shape were made by applying a pressure of 5–6 tons with a hydraulic KBR pressure machine for 120 s, using polyvinyl alcohol as binder. The binder was then heat treated at 773 K for 3 h to eliminate volatile organic compounds. At last, all GCTO pellet were sintered at 1273 K for 8 h to produce the desired ceramics.

Similarly, Co- and V-doped $Gd_{2/3}Cu_3Ti_4O_{12}$ (GCTCVO) ceramic was synthesized by adding V_2O_5 (Aldrich, Sigma, 98%) and $Co(NO_3)_2 \cdot 6H_2O$ (Merck, India, 97%).

### Material characterization

The ceramics underwent several characterization techniques to assess their properties. To confirm single-phase formation, X-ray diffractometry was performed using a Rigaku Miniflex 600 instrument from Japan. The microstructure and elemental composition of materials were analyzed using scanning electron microscopy (SEM) Nova Nano SEM 450 of Company named FEI Company of USA (S.E.A.) PTE,

LTD, and EDS machine named Team Pegasus Integrated EDS-EBSD with Octane Plus and Hikari Proof Company EDAX, Inc., respectively.

The oxidation states of the different elements present in the ceramics were determined through X-ray photoelectron spectroscopy. Pellets having cylindrical shape were prepared, with both sides coated in silver paste using ester, enabling the measurement of their dielectric and electrical properties. To analyze the real and imaginary components of impedance at different values of temperatures (in the range 303 K to 553 K) within the range of frequency 20 Hz to 2 MHz, a high-performance frequency impedance analyzer (E4980A/AL, Keysight, Malaysia) was employed.

Flow chart
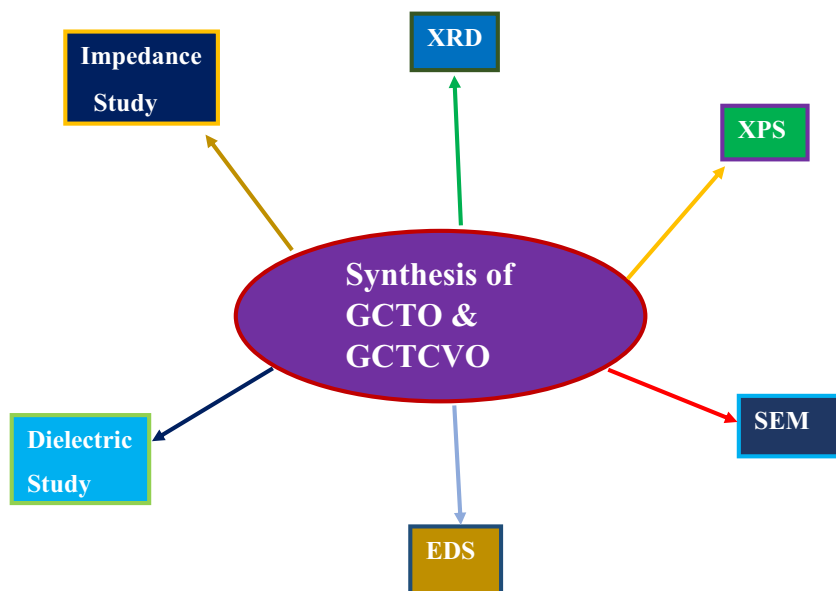
Result and discussion

X-ray diffraction analysis

Figure 1 indicates the XRD pattern of GCTO and GCTCVO ceramic material sintered at 1273 K for a duration of 8 h. It may be also observed that only single phase formation of GCTO and GCTCVO with body-centered cubic (BCC) structure was confirmed. All diffraction peaks of XRD pattern containing the different planes and patterns confirm the formation of GCTO and GCTCVO ceramic which are correctly verified with the help of JCPDS card nos. 46–0725 and 21–0140. Average crystallite sizes of GCTO and GCTCVO ceramic were evaluated using the Debye Scherer's formula [12].

$$D = k\lambda/\beta\cos\theta \tag{1}$$

In the above-mentioned equation, D indicates average crystallite size, k indicates shape coefficient ($k = 0.89$) of crystal, λ indicates wavelength of the X-ray used (1.54 Å), β indicates full width at half maximum (FWHM), and θ indicates the angle of Braggs diffraction. The image captures the significant changes in the sizes of pure GCTO crystallites brought about by Co and V doping. As the concentration of Co and V doping increased from 0 to 5%, the crystallite size decreased from 46.02 to 43.95 nm. This observation demonstrates a clear reduction in the average crystallite size with the increasing levels of Co and V doping. The primary cause of this reduction can be attributed to the distortion in the host lattice, which is induced by the presence of foreign contaminants, specifically Co^{2+} and V^{+5} ions. This distortion inhibits the nucleation and subsequent growth of GCTO NPs, ultimately leading to the decrease in

Fig. 1 XRD graph of GCTO & GCTCVO ceramic sintered at 1273 K for 8 h
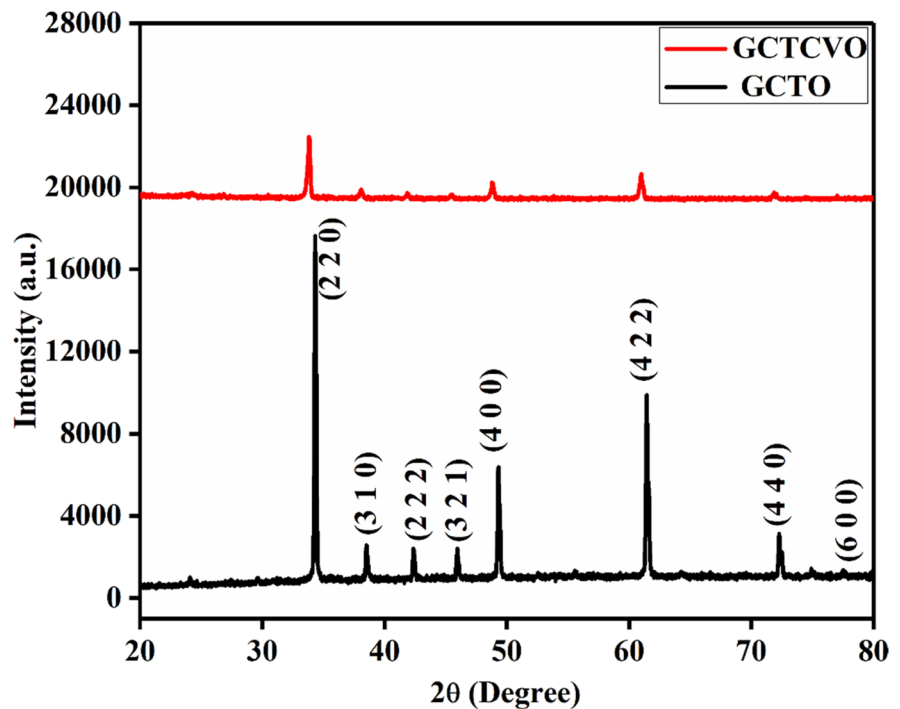
crystallite size. Furthermore, there is a noticeable decrease in X-ray diffraction (XRD) peak intensity as the concentration of Co and V increases, indicative of a decline in crystallinity. This reduction in peak intensity may be attributed to the substitutional absorption of Co and V ions into the GCTO lattice, which disrupts the orientation of the GCTO host lattice.

Additionally, variations in the ionic radii of Co, V and Ti can introduce lattice imperfections, further contributing to the decrease in peak intensity. The observed shift in peak intensities provides evidence of the successful incorporation of Co and V into the lattice, confirming the effectiveness of the doping process.

Micro-structural studies

X-ray photoelectron spectroscopy

Figure 2(a) to (f) depicts the XPS spectra of GCTCVO ceramic. XPS measurements were employed to detect the oxidation states of individual elements within these materials. In this study, carbon (C) 1 s was selected as a reference with an assigned value of 284.6 eV to account for surface charge effects. The confirmation of different metal ions, like

gadolinium (Gd), copper (Cu), titanium (Ti), cobalt (Co), vanadium (V) and oxygen (O), in GCTCVO ceramics, with the required oxidation states, was probed using XPS analysis.

XPS fitting and background subtraction were carried out using XPS-Peak 4.1 software, which revealed the presence of a gadolinium peak at 140.52 eV and 142.08 eV in GCTCVO.

Ceramics, as depicted in Fig. 2(a). In GCTCVO, the binding energy for Gd $^4dp_{3/2}$ was found to be at 146.70 eV, while for Gd $^4d_{5/2}$ the binding energies were 140.52 eV and 142.08 eV. Also, three satellite peaks may be observed at the binding energies of 153.25 eV, 158.05 eV, and 163.27 eV, respectively. Therefore, it was verified that the gadolinium ion existed in the $+3$ oxidation state within the GCTCVO ceramic. Similarly, the xps fitting of elements Cu, Ti, Co, V, and O reveals that they are present in $+2, +4, +2, +5$ and in -2 oxidation states (O.S.) in GCTCVO ceramic, respectively [13].

High-resolution scanning electron microscopy (HR-SEM) studies

Figure 3(a) to (c) and 3(d) to (f) shows the HR-SEM image of GCTO and GCTCVO ceramic, respectively,
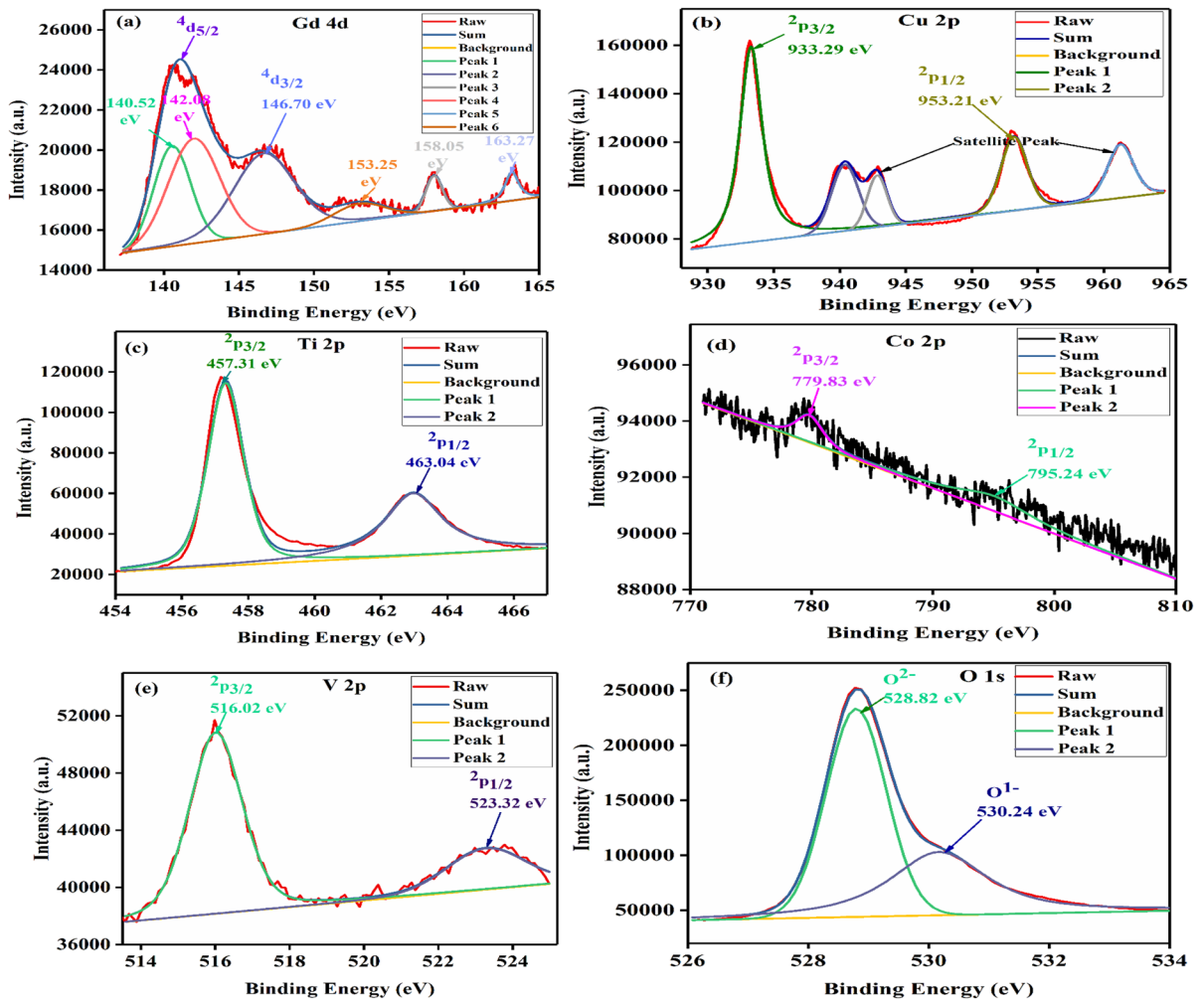
Fig. 2 XPS spectra of **a** Gd, **b** Cu, **c** Ti, **d** Co, **e** V, and **f** O, respectively, of GCTCVO ceramics sintered at 1273 K for 8 h

sintered at 1273 K for 8 h. The figures illustrate the granular morphology of grains having polygonal shapes in ceramic, and these grains are effectively separated by distinct grain boundaries.

However, shapes of all grains are faceted in GCTO and GCTCVO ceramic material. It may be clearly observed that grain morphology of GCTO and GCTCVO ceramics are almost similar in shape. No any unwanted distortion appeared in matrix of synthesized GCTO and GCTCVO ceramics. The average grain size for both synthesized materials was determined using Image J software, yielding measurements of 1.29 μm and 1.51 μm, respectively.

Energy dispersive spectroscopy

Figure 4(a)–(c) displays the energy dispersive X-ray spectroscopy (EDX) results for GCTO, while Fig. 4(d)–(f) represents the EDX outcomes for GCTCVO. The experimental analysis utilized the Team Pegasus Integrated EDS-EBSD machine model equipped with Octane Plus and Hikari Pro from EDAX Inc. The findings reveal that the primary constituents of GCTO ceramic include gadolinium, copper, titanium, and oxygen, while GCTCVO ceramic comprises gadolinium, copper, titanium, cobalt, vanadium, and oxygen.
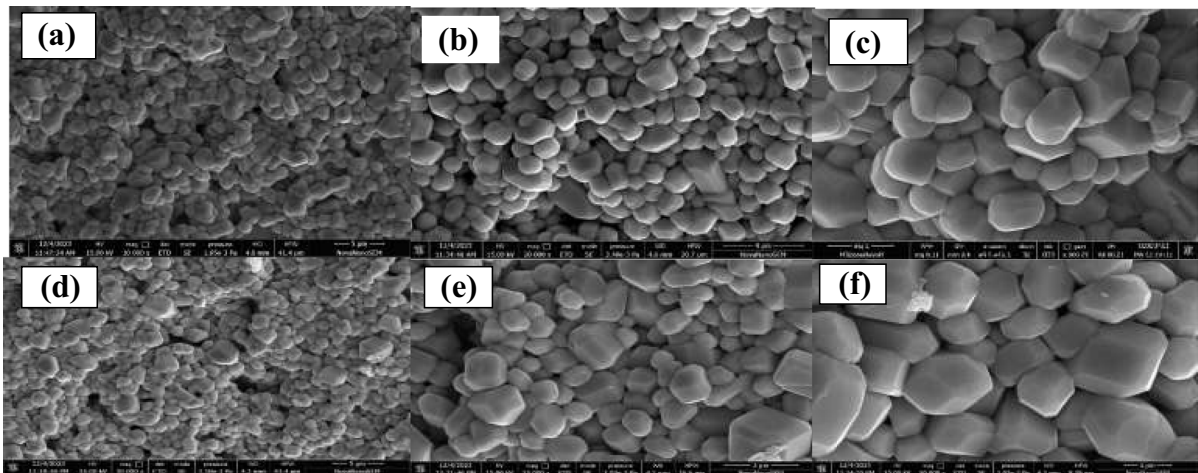
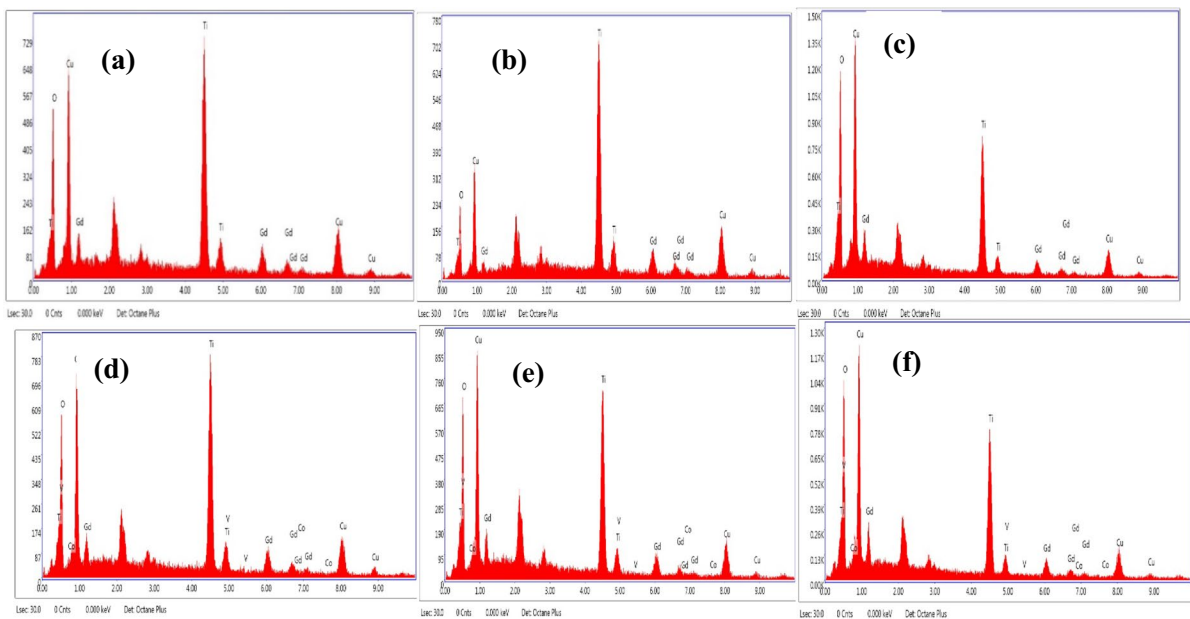**Fig. 3** **a–f** HR SEM images of GCTO and GCTCVO ceramics sintered at 1273 K for 8 h

Fig 4(a)–(c) and 4(d)–(f) exhibits EDX image of GCTO and GCTCVO ceramics at distinct positions, respectively, sintered at 1273 K for 8 h

During the EDS experiment, additional peaks of gold (Au) resulting from powder coating and carbon from chemisorbed CO_2 impurities were observed. For GCTO and GCTCVO, EDX analysis was conducted at various marked points, including the whole spectrum, spectrum 2 and spectrum 3, to elucidate the

distribution of doped cobalt (Co) and vanadium (V). Here spectrum 2 indicates grain center, while spectrum 3 indicates grain boundary.

Atomic force microscopy (AFM)

Figure 5(a)–(f) displays 2D and 3D AFM images of GCTO and GCTCVO ceramic sintered at 1273 K for 8 h, illustrating distinct grains separated by grain

Fig. 4 **a–f** EDS image of GCTO and GCTCVO ceramic sintered at 1273 K for 8 h
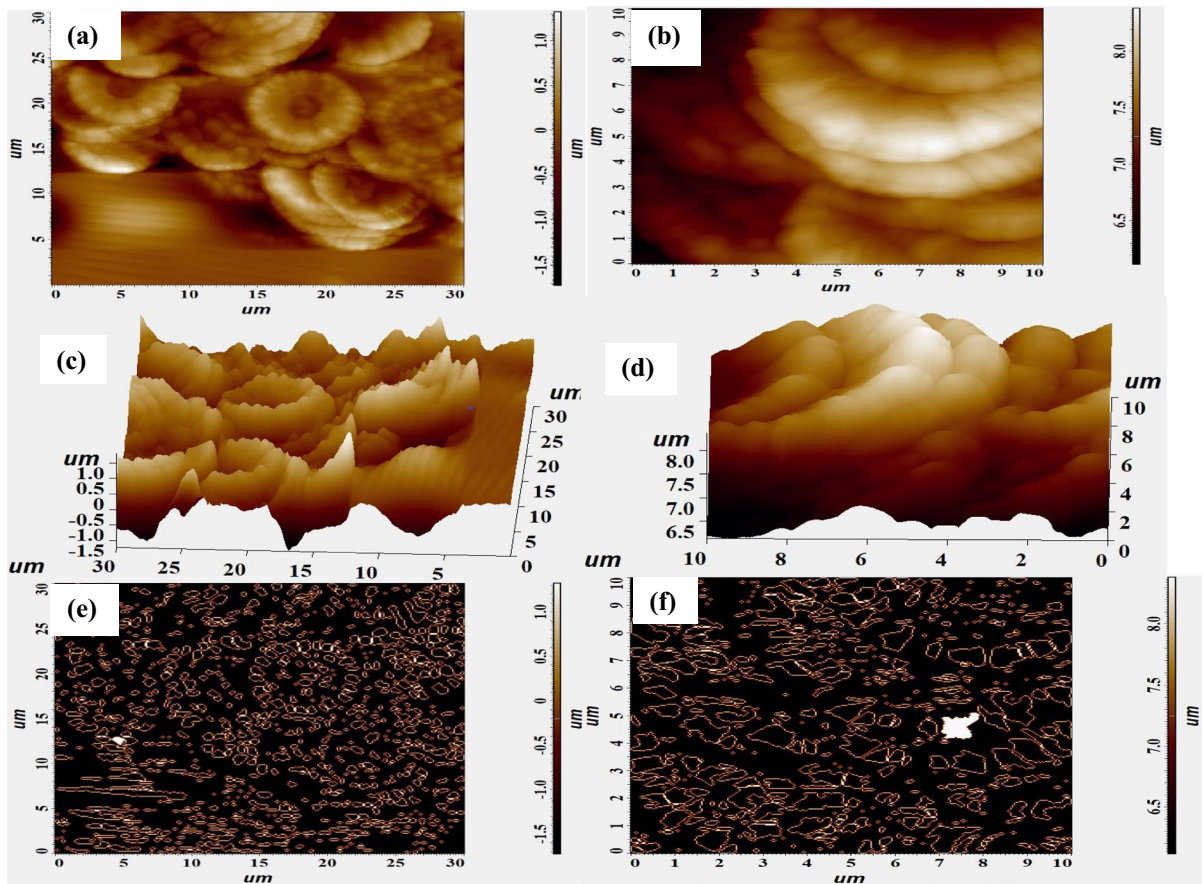
Fig. 5 **a–d** 2D and 3D image; **e**, **f** grain boundary of masked grain of GCTO and GCTCVO ceramics sintered at 1273 K for 8 h

boundaries with a sunflower like structure. The 3D representation of GCTO and GCTCVO ceramics can be observed in Figs. 5(c) and 6(d). Utilizing Nova software, the average roughness (Ra) and root mean square (RMS) for the 3D images were calculated, resulting in values of 0.278 μm and 0.370 (rms) μm for GCTO ceramic and 0.278 μm and 0.345 (rms) μm for GCTCVO ceramic, respectively.

Dielectric studies

Figure 6(a) and (b) illustrates the temperature-dependent behavior of the real part (ε') of the dielectric constant for GCTO and GCTCVO ceramics, respectively, across a temperature range of 303 to 553 K, while Fig. 6(c) and (d) clearly depicts the trend of dielectric constant (ε') as a function of frequency. In the higher frequency range, extending up to 1 MHz, the dielectric constant remains constant due to the occurrence of rapid periodic reversal of the electric field. At a temperature of 303 K and a frequency of 1 kHz, the dielectric constant was measured at 303 and 76 for GCTO and GCTCVO ceramics, respectively. Figure 6(a) and (b) further elucidates the behavior of the real part (ε') of GCTO and GCTCVO ceramics at selected frequencies ranging from 1 kHz to 1 MHz. The dielectric constant remains constant up to 350 K at all measured frequencies. Beyond this temperature, there is an increase in the dielectric constant with rising temperature, primarily at lower frequencies. However, at 100 kHz and 1 MHz, the dielectric constant exhibits minimal sensitivity to temperature variations and remains constant due to the occurrence of rapid periodic reversal of the electric field. It can be also observed that dielectric property decreases with increase in frequency at a particular temperature, as shown in Fig. 6(c) and (d).
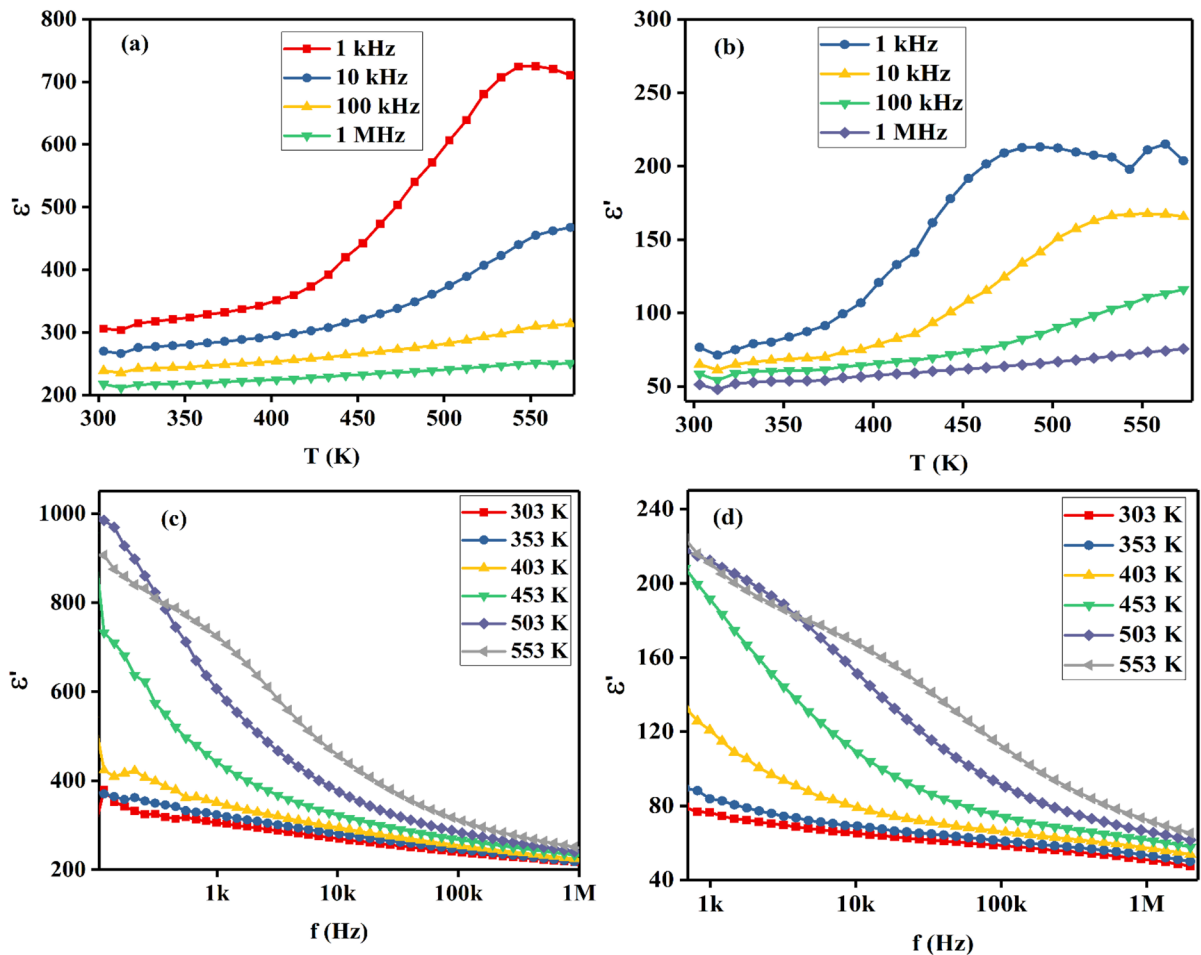
Fig. 6 a, **b** Variation of dielectric constant with temperature; **c**, **d** variation of dielectric constant with frequency of GCTO and GCTCVO ceramics, respectively, sintered at 1273 K for 8 h

The temperature-dependent behavior of tanδ closely mirrors that of the dielectric permittivity, providing evidence for the presence of Maxwell–Wagner relaxation phenomena. At 303 K the values of tanδ for GCTO and GCTCVO ceramics were observed to be 0.08 and 0.13, respectively, for all measured frequency, as shown in Fig. 7(a) and (b). It may be also observed that the value of tanδ is constant up to 383 K and 334 K at all frequencies, after that the value of tanδ increases with increase in temperature.

The dielectric loss steadily diminishes with increasing frequency in the lower frequency ranges, up to 100 kHz, and maintains a constant value in the higher frequency domains at all temperature, as shown in Fig. 7(c) and (d). This observed trend

in tanδ serves as evidence for the presence of Maxwell–Wagner relaxation phenomena. [14–16]

Impedance analysis

Figure 8(a) and (b) displays Nyquist plots illustrating the complex impedance relationship between Z'' and Z' for GCTO and GCTCVO ceramic sintered at 1273 K for 8 h. These plots unveil temperature-induced effects on the characteristic impedance spectrum. Below 403 K, the Nyquist plot manifests a straight line with a substantial slope, indicating the sample's insulating behavior. The slope's gradient decreases between 403 and 453 K. Beyond 503 K, the linear
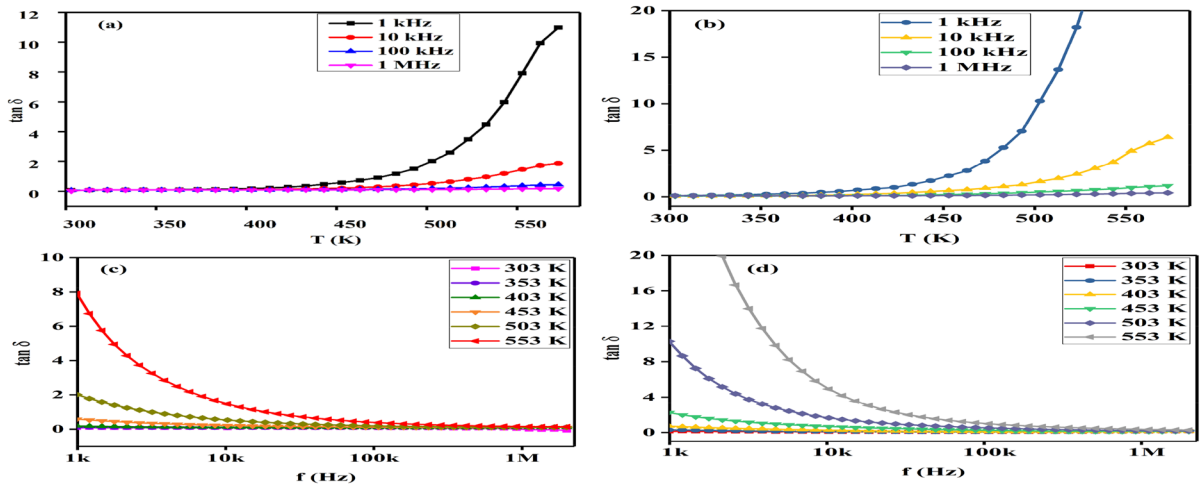
Fig. 7 a, **b** Variation of dielectric loss with temperature; **c**, **d** variation of dielectric loss with frequency of GCTO and GCTCVO, ceramics, respectively, sintered at 1273 K for 8 h
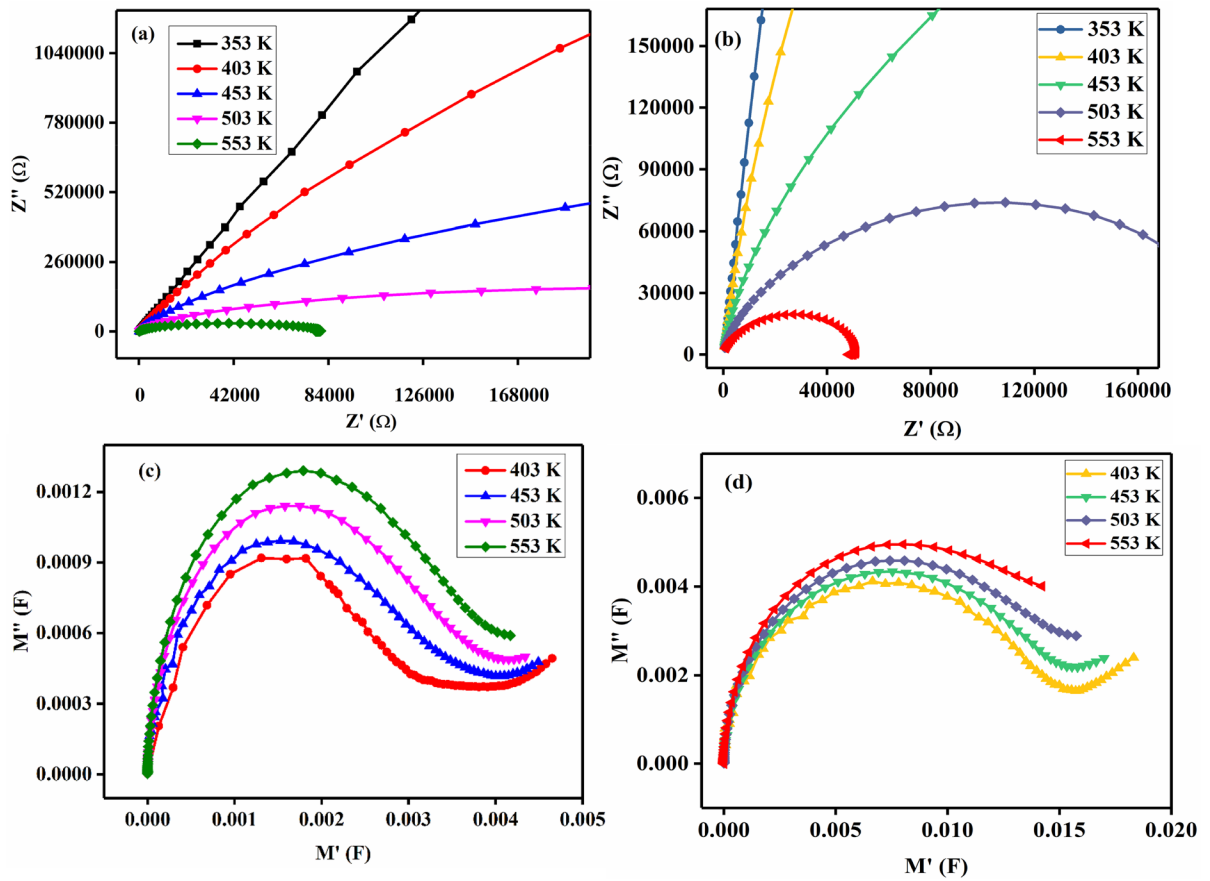
Fig. 8 a, **b** Nyquist plot; **c**, **d** Cole–Cole plot of GCTO and GCTCVO ceramics, respectively, sintered at 1273 K for 8 h

Table 1 The value of R_g and R_{gb} at different temperatures obtained from Nyquist plot for GCTO and GCTCVO ceramic

Sample	Temperature (K)	Rg (Ω)	Rgb (Ω)
GCTO	353 K	34	———
	403 K	21	———
	453 K	10	3.97×10^6
	503 K	8	4.40×10^5
	553 K	5	8.80×10^4
GCTCVO	353 K	161	———
	403 K	123	———
	453 K	27	1.15×10^6
	503 K	———	1.99×10^5
	553 K	———	5.15×10^4

response transitions to a semicircular arc, signifying increased sample conductivity. These arcs manifest in the high-frequency range with diminished impedance values as the temperature increases. The presence of both low- and high-frequency semicircular arcs is explained through an equivalent electrical circuit model. Generally, three semicircles were observed, representing the combined impact of grain, grain boundary, and electrode contributions across the higher and lower frequency range. [17–19]

The presence of a low-frequency semicircular arc is attributed to grain boundary effects arising from the parallel combination of Rgb and Cgb. On the other hand, the high-frequency semicircular arc is linked to the bulk properties of the material, resulting from the parallel combination of R_g and C_g. The values of Rgb and Rg at different temperatures are given in Table 1.

Figure 8(c) and (d) depicts the modulus plot for undoped and doped GCTO ceramics at different temperatures. Two distinct arcs can be clearly discerned across the entire measured frequency range in both ceramics. Subsequent arc represents the contribution from grains. It is noteworthy that an elevation in temperature results in a decrease in the capacitance of both grains (Cg) and grain boundaries (Cgb). The trend depicted in the figure demonstrates that the capacitance of both grains and grain boundaries increases with higher dopant concentrations.

Dielectric relaxation

The dielectric relaxation behavior of GCTO and GCTCVO ceramic compound sintered at 1273 K for 8 h is shown in Fig. 9(a) and (b). The imaginary Z'' data was graphed using normalized coordinates, specifically plotting Z''/Z'' max against f/f_{max}. If the impedance relaxation peaks could be amalgamated into a single overarching curve, it would imply that the duration of relaxation remains unaffected by changes in temperature. However, this hypothesis was not validated, as the relaxation peaks at different temperatures did not converge into a unified master curve, as depicted in Fig. 9(a) and (b). This implies that the scaling behavior of Z'' indicates that the distribution of relaxation time is not influenced by temperature and illustrates a non-Debye (Maxwell)-like relaxation [20].

Electrical conductivity

The plot depicting $\log\sigma$ against $1000/T$ for GCTO and GCTCVO ceramics, sintered at 1273 K for 8 h, is presented in Fig. 10(a) and (b). It is evident that the

Fig. 9 a, b Nature of dielectric relaxation of GCTO and GCTCVO ceramics, respectively, sintered at 1273 K for 8 h
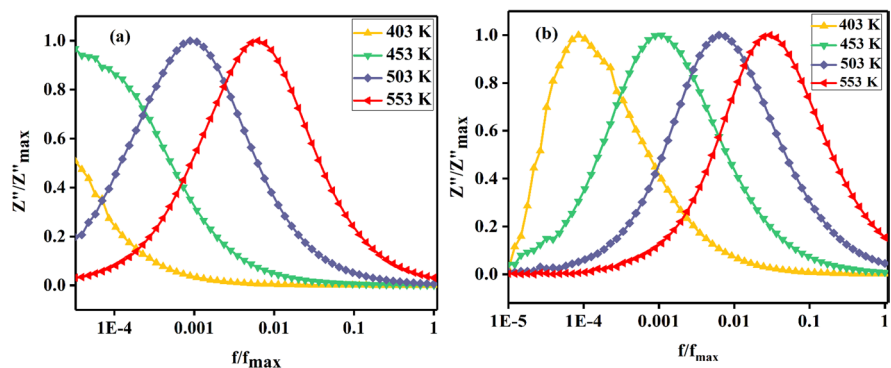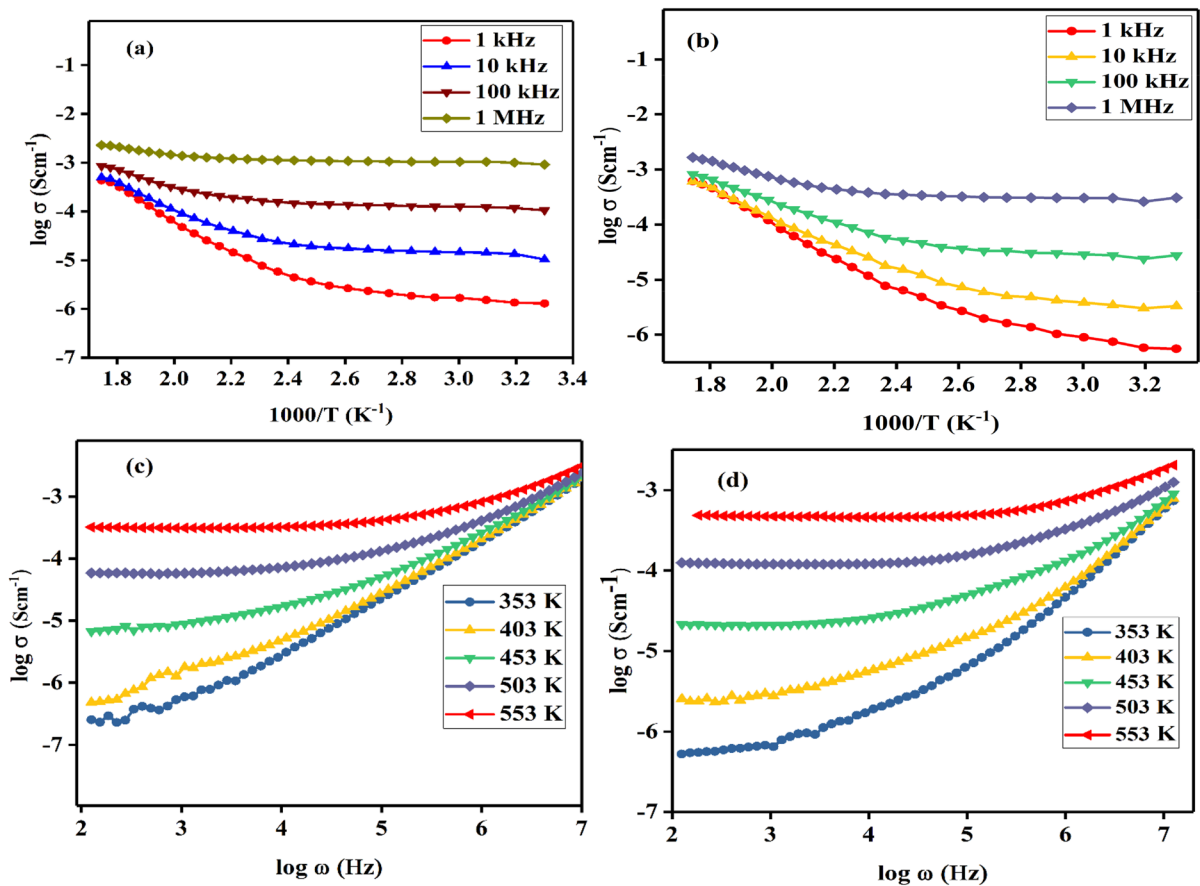
Fig. 10 **a**, **b** variation of conductivity with inverse of temperature; **c**, **d** frequency dependent behavior of AC conductivity of GCTO and GCTCVO ceramics, respectively, sintered at 1273 K for 8 h

$\log\sigma$ values decrease as the temperature decreases, indicating adherence to the Arrhenius law. The activation energies, observed at various frequencies for GCTO and GCTCVO at lower temperatures, are found to be 0.62 eV, 0.43 eV, 0.23 eV, 0.12 eV and 0.65 eV, 0.50 eV, 0.38 eV, 0.25 eV, respectively. It is noteworthy that the activation energy gradually decreases with increasing frequency for both GCTO and GCTCVO ceramics, maintaining constancy at higher frequencies.

The Jonscher power law, represented as

$$\sigma(\omega) = \sigma_0 + A\omega^s, \tag{2}$$

The context where A is a constant and s represents the power law exponent describes the frequency-dependent conductivity. The power law exponent (s) was determined by analyzing the curve for GCTO and GCTCVO

at different temperatures (353 K, 403 K, 453 K, 503 K, and 553 K) shown in Fig. 10(c, d). It was noted that value of s decreases as the temperature increases, consistently staying below 1 at every temperature level.

The conduction mechanism in these ceramics is governed by the thermally activated hopping of charge carriers between two sites, separated by an energy barrier at the grain boundary. The dielectric conduction process is temperature dependent and entails the hopping of charge carriers [21, 22].

Conclusion

GCTO and GCTVO ceramic nano-particles were synthesized utilizing a cost-effective chemical route. XRD pattern confirms single-phase formation of $Gd_{2/3}Cu_3Ti_4O_{12}$

(GCTO) and Co–V-doped $Gd_{2/3}Cu_3Ti_4O_{12}$ (GCTCVO) ceramic. XPS analysis verified the correct oxidation states of various elements. Elemental composition was determined using EDS. The dielectric constant of GCTO ceramic reached its peak at 726, measured at 545 K and 1 kHz, while it reached its peak at 217, measured at 563 K and 1 kHz for GCTCVO. It was also observed that both ceramic shows Maxwell relaxation behavior. The tangent loss value of the GCTO and GCTCVO ceramic was noted as 0.08 and 0.13 at 304 K and all measured frequency.

Author contribution   All authors participated in the initiation and design of the study. Each author has thoroughly reviewed and granted approval for the final manuscript.

Data availability   The research data was not disclosed.

Declarations

Competing interests   The authors declare no competing interests.

References

1. Swatsitang E, Anuson Niyompan A (2013) Giant dielectric, low dielectric loss and non-ohmic properties of nanocrystalline $CaCu_3Ti_4O_{12}$.J. Mater Sci Mater 24:3514–3520
2. Brizé V, GruenerG WJ, Fatyeyeva K, Tabellout M, Gervais M, Gervais F (2006) Grainsize effects on the dielectric constant of $CaCu_3Ti_4O_{12}$ ceramics. Mater Sci Eng B 129:135–138
3. Jesurani S, Kanagesan S, VelmuruganR TC, Sivakumar M, Kalaivani T (2011) Nanoparticles of the giant dielectric material, calcium copper titanate from a sol–gel technique Mater. Lett 65:3305–3308
4. Luo F, He J, Hu J, Lin YH (2010) Electric and dielectric behaviours of Y-doped calcium copper titanate. J Am Ceram Soc 93:3043–3045
5. Kumar RA, Kumar SN, Kumar AS, Laxman S, Mandal KD (2012) Effect of tantalum substitution on microstructures and dielectric properties of calcium copper titanate ($CaCu_3Ti_4O_{12}$) ceramic. Mater Sci Eng: B 177:1213–1218
6. Mu C, Zhang H, He Y, Liu P (2010) Influence of temperature on dielectric properties of Fe-doped CaCu3Ti4O12 ceramics. Phys B: Condens 405:386–389. https://doi.org/10.1016/j.physb.2009.08.093
7. Li M, Feteira A, Sinclair DC (2006) Influence of Mn doping on the semiconducting properties ofceramics. App Phys Lett 88:232903. https://doi.org/10.1063/1.2200732
8. Cai J, Lin YH, Cheng B (2007) Dielectric and nonlinear electrical behaviors observed in Mn-doped ceramic. App Phys Lett 91:252905. https://doi.org/10.1063/1.2825472
9. Ribeiro WC, Araujo RGC (2011) The dielectric suppress and the control of semiconductor non-Ohmic feature of by means of tin doping. App Phys Lett 98:132906. https://doi.org/10.1063/1.3574016
10. Makcharoen W, Tontrakoon J (2010) Effect of cesium and cerium substitution on the dielectric properties of CaCu3Ti4O12 ceramics. Ceram Int 38. https://doi.org/10.1016/j.ceramint.2011.04.051
11. Subramanian MA, Li D, Duan N (2000) High dielectric constant in ACu3Ti4O12 and ACu3Ti3FeO12 phases. J Solid State Chem 151. https://doi.org/10.1006/jssc.2000.8703
12. Holzwarth U, Gibson N (2011) The Scherrer equation versus the "Debye-Scherrer equation." Nat Nanotechnol 6:534. https://doi.org/10.1038/nnano.2011.145
13. Kumar A, Kumar V, Verma MK, Rai VS (2023) Jena Biswajit Dielectric and electrical properties measurement of BCTO and Co & V-doped BCTO synthesized via semi-wet route method. J Mater Sci Mater Electron 34:1755
14. Rai AK, Singh NK (2012) Effect of tantalum substitutions on microstructures and dielectric properties of calcium copper titanates (CaCu3Ti4O12) ceramic. Mater Sci Eng B 177:1213–1218
15. Liu J, Duan CG, Yin WG (2004) Large dielectric constant and Maxwell-Wagner relaxation in $Bi_{2/3}Cu_3Ti_4O_{12}$. Phys Rev B 70:144106
16. Lu Z, Wang G, Bao W, Li J (2022) Superior energy density through tailored dopant strategies in multilayer ceramic capacitors. Energy Environ Sci 13(9):2938–2948
17 Irvine JT, Sinclair DC, West AR (1990) Electroceramics: characterization by impedance Spectroscopy. Adv Mater 2(3):132–138
18. WangY LH, Yan T, Zhao J, Li J, Guo S, Sun S, Sun R, Lu Z, Wang D (2022) significantly reduced conductivity in strontium titanate-based lead-free ceramics by excess bismuth. Mater Lett 309:131453
19. Rayssi C, Jebli M, Bouzidi S, Dhahri J, Belmabrouk H, Bajahzar A (2022) Impedance analysis and modulus behavior of CaO.85Er0.1Ti(1-x)Co4x/3O3 (x=0.15and 0.20 ceramic prepared by sol-gel reaction. App Phys A 128:435
20. Jianjun L, Chun-Gang D, Wei-Guo Yin, Mei WN, Smith RW, Hardy JR (2004) Large dielectric constant and Maxwell-Wagner relaxation in $Bi_{2/3}Cu_3Ti_4O_{12}$. Phys Rev B 70:144106
21. Leiand Z, Zhong-Jia T (2004) Polaron relaxation and variable-range-hopping conductivity in the giant-dielectric-constant material $CaCu_3Ti_4$ O_{12}. Phys Rev B 70:174306
22. Laxman S, Lokeswararao D, Rajasekhar B (2023) Low-costflame synthesized La 2/3 Cu 3 Ti 4 O 12 electro-ceramic and extensive investigation on electrical, impedance, modulus, and optical properties. Ceram Int 49(13):21795–21803